Au release layer development for high-angular resolution, replicated full shell X-ray optics

Danielle N. Gurgew[a,b], Srikanth Panini Singam[a], David D. Smith[b], Stephen D. Bongiorno[b], David A. Banks[b], Jessica A. Gaskin[b], Nicholas E. Thomas[b], Brian D. Ramsey[b], and Kirtan P. Dixit[b,c]

[a]Universities Space Research Association, Science and Technology Institute, Huntsville, AL, 35805 United States
[b]NASA Marshall Space Flight Center, Huntsville, AL, 35812 United States
[c]Oak Ridge Associated Universities, Oak Ridge, TN, 37830 United States

ABSTRACT

The X-ray group at NASA Marshall Space Flight Center is developing replicated full shell X-ray optics for future mission concepts with the goal of achieving sub-arcsecond angular resolution. One of the electroforming steps that may contribute significantly to resolution degradation of the mirror shell is the shell separation from the mandrel. Traditionally, a passivation layer has been used between the mandrel and the NiCo shell to enable shell release, resulting in the required moderate angular resolution mirror shells. However, as resolution requirements become more stringent, improvements to this process must be investigated. To this end, we present the application of gold release layers for full shell optics designed to improve the optic fabrication process and reduce azimuthal errors.

MSFC sputtered gold coatings are first optimized and characterized via X-ray reflectometry (XRR) measurements, atomic force microscopy (AFM), optical profilometry, and adhesion testing. Initial replication studies conducted on flat coupons are presented along with a comparison to other replicants fabricated using a passivation layer. To validate the Au release layer for grazing incidence geometries, sputtered gold coatings were deposited onto a mandrel from which full shell optics are replicated. We report on the shell circularity and X-ray performance and compare the results to that of an identical optic fabricated with a passivation layer.

Keywords: Nickel X-ray optics, full-shell, release layer, gold coatings

1. INTRODUCTION

Alongside the development of high-resolution, full-shell replicated X-ray optics, NASA Marshall Space Flight Center (MSFC) is also pursuing the development of advanced thin film coatings. As part of this research program, we investigate thin release layers to enable smoother shell release from the underlying mandrel during fabrication. It is hypothesized that the release stresses contribute to the shell's axial and azimuthal deformations, which distort the figure and reduce overall performance due to half-power diameter (HPD) degradation. As the angular resolution requirements for nickel replicated optics become more stringent, these release errors become more pronounced and must be addressed in the overall effort of improving the full-shell fabrication process.

Over the past three decades, MSFC has developed and advanced the electroformed nickel replication (ENR) process through both sub-orbital and on-orbit flight projects including the HERO(S) balloon program,[1],[2] FOXSI sounding rocket missions,[3],[4] ART-XC,[5] and IXPE.[6] The typical process consists of the following steps: electroless nickel-coated aluminum mandrels are diamond-turned to create high-precision optical prescriptions and super polished to provide sub-nanometer surface roughness; these mandrels are then passivated to form an oxide layer on the surface using potassium dichromate to assist with shell separation; the passivated mandrel is submerged into the electroforming bath, onto which the shells are grown. The shell is separated from the mandrel via

Further author information: (Send correspondence to D.N.G.)
D.N.G.: E-mail: danielle.n.gurgew@nasa.gov, Telephone: 1 256 961 7689

differential thermal contraction of the mandrel relative to the shell, the release of which is enabled by the passivation layer.

Recent advancements in mandrel polishing at MSFC has enabled near sub-arcsecond axial performance;[7] however, replicated shells still under perform relative to this. Most of the errors for optical figure in the shells arise from non-circularity which affects overall imaging performance, limiting the angular resolution.[8] These circularity errors must be addressed as angular resolution requirements move toward the sub-arcsecond level. It is hypothesized that as the shell releases from the mandrel, it does so in a non-even manner, resulting in local stress concentrations which in turn can cause microyielding of the shell material. Microyielding is a parts per million plastic deformation that occurs at much lower stresses than the engineering yield. As such, efforts to improve the shell release process include utilizing a gold release layer in place of the traditional passivation layer. The aim is to develop a gold release layer to provide lower adhesion to the NiP mandrel while the Ni shell forms a metallic bond to the gold. Therefore, the gold enables a much smoother release from the mandrel while staying bonded to the shell surface. This method has been used by MSFC and other groups in the past, but has yet to be comprehensively studied as a path toward achieving sub-arcsecond imaging performance.

MSFC had previously studied Au layers for replicated NiCo optics,[9] first passivating the mandrel surface for release then depositing an Au layer on the passivated mandrel for enhance X-ray reflection. As this process development became more mature and other methods of coating the inside of full shell replicated optics became available (RF sputtered Ir thin films)[10],[11] the Au layer was removed from the fabrication process. As the angular resolution requirements have become more stringent, the dichromate release has proven to not be sufficient enough to achieving these imaging goals. Therefore, a program for further study and optimization of Au thin films as a release layer has been re-established within MSFC.

XMM-Newtwon, ESA's flagship X-ray telescope, utilizes Ni replicated optics technology including Au release layer during fabrication to achieve ∼15" angular resolution in the standard X-ray band[12].[13] Quantifying how well the Au release layer mitigates certain release stresses has yet to be thoroughly investigated. Some studies[14][15] have detailed the gold release thickness optimization as a function of coating quality (e.g. surface roughness and density). Other studies highlight the adhesion properties of the Au release layer on NiP mandrel surface and how this could potentially be mitigated via a diamond-like carbon barrier layer.[16] TiN has been proposed as an alternative material that remains on the mandrel surface after many replications.[17] However, the impact of these release layers on the shell's figure, including both circularity and axial deformation, has not been rigorously quantified and is considered to be a significant parameter impacting the imaging quality of these optics. As we move to achieve sub-arcsecond replicated full shell optics, understanding how the shell release impacts these metrics and how we can minimize them (through Au release layer development) is now at the forefront of our investigative research.

2. AU RELEASE LAYER OPTIMIZATION AND CHARACTERIZATION

2.1 Au Coating Parameter Optimization

MSFC's thin film coating laboratory includes an in-house DC magnetron sputtering system,[18] that houses three 2 in diameter cathodes which move underneath a substrate holder that rotates about it's axis mounted from the lid of the chamber. One of the three cathodes has been commissioned for use in the initial testing of proof of concept sputtered Au films for release layer applications. Calibration of gold deposition rates and coating parameters such as thickness, density, and roughness were conducted on 2 in diameter super-polished silicon wafers. DC magnetron sputtering typically results in high-adhesion, low roughness, and high density coatings. This process need to be optimized for Au release layer applications in order to reduce the coating adhesion while maintaining roughness and near bulk density.

Argon gas pressure and cathode power were varied for coatings in two distinct groups for Au films around 500 Å. Group 1 coatings were deposited at a constant power of 150 W with a variable Ar gas pressure from 3 to 20 mTorr. Group 2 coatings were deposited at a constant gas pressure of 3 mTorr with a variable cathode power from 25 to 150 W. Table 1 summarizes the deposition parameters and best fit[19] coating parameters from XRR of each of these coatings. An in-house reflectometer system at 8.040 keV was used for these measurements and is described in detail in other publications.[20] The average coating thicknesses are 500 Å ± 26.23 and 524 Å ±

15.85 for Group 1 and 2, respectively. Optimum coating parameters were selected based on maximum Au density while maintaining reasonable surface roughness (less than 9 Å). Group 1 optimized parameters are defined as 15 mTorr, 150 W (Au SLTest7), and Group 2 optimized parameters are defined as 3 mTorr, 50 W (Au SLTest11). While these process parameter combinations provide high density and moderate surface roughness, the main concern for the Au release layer is the adhesion of these coatings to the mandrel surface. Surface roughness of the Au layer will be most significantly impacted by the mandrel surface quality.

Table 1: Au Layer Optimization Study: Coating Parameters

	Coating ID	Au Power (W)	Gas Pressure (mTorr)	h (Å)	ρ (g/cm^3)	σ (Å)
Group 1	Au SLTest1	150	3	513.75	18.95	6.49
	Au SLTest2	150	5	530.94	18.98	7.88
	Au SLTest3	150	10	522.00	18.58	7.28
	Au SLTest4	150	15	489.31	19.30	7.61
	Au SLTest7	150	17	469.57	19.30	7.51
	Au SLTest5	150	20	463.65	19.29	10.15
Group 2	Au SLTest1	150	3	510.62	18.95	6.49
	Au SLTest8	100	3	513.75	19.04	7.87
	Au SLTest9	75	3	384.25	19.24	6.71
	Au SLTest10	75	3	519.16	19.21	7.62
	Au SLTest11	50	3	521.69	19.30	6.50
	Au SLTest12	25	3	551.67	18.93	8.03

2.2 Au Coating Adhesion Testing

Evaluation of the optimized coating adhesion to the mandrel surface material, super polished NiP, is critical to understanding the effectiveness of the Au release layer relative to the potassium dichromate. The optimized Au coatings are deposited onto a cleaned NiP plated "coupon" test flats which are polished in the same process as the mandrels to achieve several angstrom-level surface roughness. After coating, pull tests using the Defelsko PosiTest AT adhesion tester[21] are performed to determine order of magnitude adhesion strengths for each of the coatings. Au coating parameters from Group 1 optimization results were used to coat Coupon Test 1 (150 W, 17 mTorr gas pressure) while the optimized coating parameters from Group 2 were used to coat Coupon 2 (50 W, 3 mTorr gas pressure).

The adhesion of the gold layer from Coupon Test 1 was found to be approximately 25 $\pm$ 7 psi with confirmed full delamination using a tape test. In contrast, the adhesion of Coupon Test 2 was found to exceed that of the limits of the pull tester apparatus (which is 3000 psi). Additionally, a tape pull test gave a null result with no visible delamination. See Figure 1 for photos of the test setup and tape test results. Conclusions from this study indicate higher gas pressure results in high-quality Au thin films on the order of 500 Å with relatively low adhesion (Coupon Test 1). Historically, MSFC has reported an adhesion limit of 100 psi for the potassium dichromate release layer such that shells still achieve moderate angular resolution. Therefore, the coating parameters and adhesive properties of the sputtered Au coating from Coupon Test 1 are identified as the optimal process parameters for the Au release layer development and testing for this work.

2.3 Au Replicant Fabrication: Au vs. Passivation

Proof concept studies on flat samples include depositing the optimized Au release layer onto NiP coupons, plating onto the coated coupon and performing a release in the typical fashion. Pre-plating, the coated coupon was measured with XRR to verify Au layer properties. Post-plating, the resulting flat replicant is assessed for surface roughness using AFM and optical profilometry (Zygo New View) to characterize how the release impacts

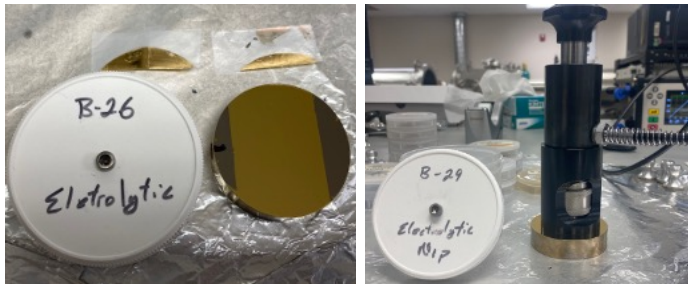

Figure 1: Left: Tape test result from Coupon Test 1 with full delamination demonstrated. Right: Adhesion tester setup for Coupon Test 2. No delamination of coating was observed via pull test or tape test.

the optical surface. The replicant is also measured on a Zygo Fizeau interferometer to assess surface figure. The bare coupon is also measured in this fashion as a baseline reference. These results are then compared to a second replicant made from the same coupon using the traditional fabrication process involving a passivation layer instead of gold. Both metrics, surface roughness and replicant figure, are directly compared.

Replicant 1 was fabricated on the G12 NiP coupon with the optimized 500 Å Au release layer and is referred to as G12-S05. XRR measurements of the Au layer pre-plating were conducted and analyzed. The resulting best fit parameters are as follows: coating thickness, h, of 510.8 Å, density of 18.75 g/cm^3, and surface roughness of 7.14 Å. G12-S05 is 350 μm thick deposited using electroplating parameters of 13 ASF and +0.4 ksi. The replicant released within $\sim$30 s post bath with no cold water rinse needed to assist with separation. Figure 2 shows the G12 coupon and G12-S05 post-release along with the XRR data of the pre-plated Au layer on the G12 coupon. Resulting surface roughness measurements from both AFM and New View measurements indicate a slight increase in the G12-S05 replicant surface compared to the pre-coat G12 coupon surface. See Figure 3 for images of G12-S05 surface. Roughness values of 4.53 Å and 5.28 Å (New View and AFM, respectively) of the replicant, while not high compared to the coupon surface roughness of 3.52 Å and 3.98 Å (New View and AFM, respectively), could be improved through further refinement of the Au layer thickness and/or cathode power and will be reviewed for future studies.

Figure 2: Left: G12 coupon post-release in plating bath fixture. Middle: G12 coupon with released G12-S05 replicant. Right: XRR data of Au coating on G12 coupon with IMD fit and extracted coating parameters.

Surface figure measurements of G12-S05 were conducted on the Zygo Fizeau interferometer with a 4in aperture and transmission flat. The replicant was placed on a semi-kinematic mount positioned flat on the optical bench such that a 45 degree fold mirror reflects the laser onto the sample surface (See[22] for further details). Both the G12 coupon and G12-S05 were measured with this system to provide figure measurements for direct comparison. Two orthogonal cross sections of G12-S05 were also taken to highlight the convex figure. The resulting surface figures are shown in Figure 4. The peak-to-valley (PV) parameter of the G12 coupon and G12-S05 are 0.626 μm and 16.673 μm, respectively. The G12 coupon exhibits a relatively flat surface while the replicant figure is fully convex, indicating compressive residual stress within the part.

For comparison to the traditional fabrication method, two replicants were made off the G12 coupon using

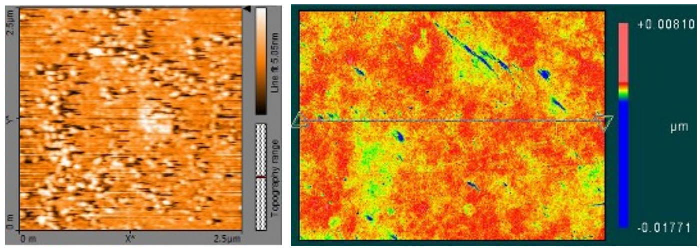

Figure 3: Left: Example AFM topography map of 2.5 μm^2 area of G12-S05 replicant surface with an rms surface roughness of 5.28 Å (average of 5 scans). Compare to the bare G12 coupon AFM roughness value of 3.98 Å. Right: Optical profilometry topography map (0.52mm x 0.7mm) of G12-S05 replicant with rms surface roughness of 4.53 Å (average of 5 scans). Compare to the bare G12 coupon New View roughness value of 3.52 Å.

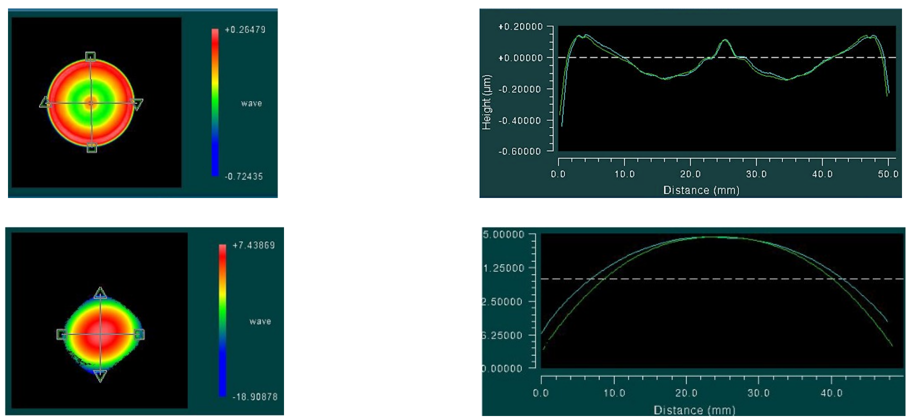

Figure 4: Top row: G12 bare coupon figure measured with Zygo Fizeau and corresponding orthogonal cross sectional profiles with PV value of 0.626 μm. Bottom row: G12-S05 replicant figure with PV of 16.673 μm and cross sectional profiles, indicating axially symmetric residual stress in the replicant. Y axis units are μm.

the passivation layer in place of Au: G12-S01 and G12-S02. The figure of these replicants were measured and are shown in Figure 5. Edge flaring is seen in the cross sections for both coupons (a repeatable result) that could indicate micro-yielding of the NiCo during release. The overall convex shape of the passivated replicants implies a residual tensile stress, opposite to that of G12-S05. Although the shapes cannot be directly compared from G12-S05 to -S01 and -S02 due to opposite stress, the edge flaring was not present in G12-S05, giving some indication that the Au release layer may result in less micro-yielding during release. To further investigate this hypothesis, the gold release layer is applied to the full shell geometry and compared with the traditional process, keeping the NiCo plating stress constant for each of the shell platings.

3. FULL SHELL FABRICATION WITH AU RELEASE LAYER

A small mandrel (referred to as the 62 mm mandrel) was selected to perform the first full shell release with the optimized gold layer due to limited space available within the DC magnetron sputtering chamber. The 62 mm mandrel is 1/10th the scale of the inner optic on Chandra with an intersection diameter of 62 mm and a length of approximately 7 in without the two end caps. The sputtering chamber was retrofitted with a custom fixture on which the mandrel rotated during deposition to ensure azimuthal coating uniformity. The process parameters are the same as those used for G12-S05 (17mTorr, 150W, 500 Å). Figure 6 shows the key steps in the full shell release layer fabrication process. The mandrel is coated in the DC magnetron sputtering system with 500 Å of gold, configured for plating with custom gaskets and end shields, placed in the electroforming bath - achieving 350 μm thick NiCo plating, and the resulting shell is released via temperature differential. Two shells of identical

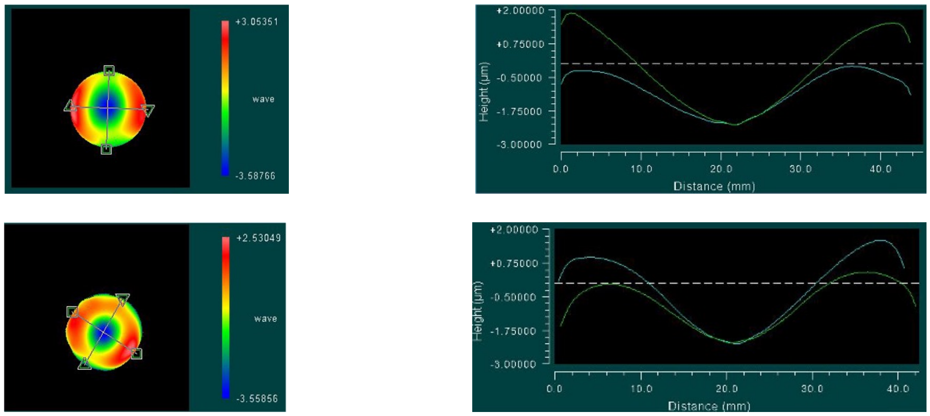

Figure 5: Top row: Surface figure and cross sectional profiles of G12-S01 with measured PV of 4.203 μm. Bottom row: Surface figure and cross sectional profiles of G12-S02 with measured PV of 3.853 μm. Both replicants were fabricated using the passivation layer. Flaring at the ends of the replicants indicate possible microyielding of the NiCo as a result from the release.

thickness and plating stress were fabricated for this comparison study: the gold release layer shell 62mm-S02 and the passivated shell 62mm-S03.

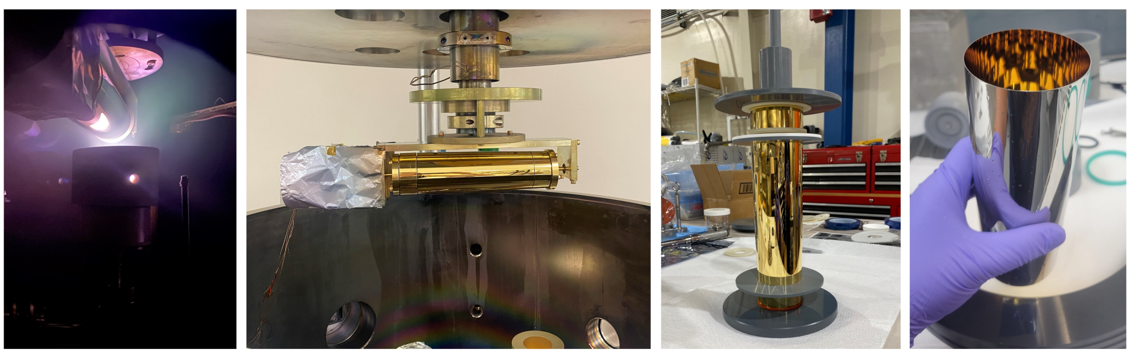

Figure 6: From left to right: Au deposition process on rotating 62 mm mandrel. Au-coated mandrel on rotatory fixture in vacuum chamber. Coated 62 mm mandrel with plating gaskets and shields just before submersion into plating bath. Released Au-coated 62 mm shell, S02.

3.1 Circularity Measurements

The figure error of full shell optics is dominated by circularity or out-of-roundness errors, most of which occur during shell release.[7] To characterize any existing improvement in optical performance of full shell optics utilizing an Au lease layer relative to a passivation layer, shell circularity as a function of axial position must be measured precisely. A custom circularity station setup[23] was utilized for this work. The shell is suspended from a precision motor-driven mount system thereby minimizing gravity-induced distortions. Displacement sensors operating at sub-μm precision are mounted at three distinct axial positions such that as they rotate around the suspended shell, the azimuthal variations of the optic are measured and recorded. The local slope profiles at each azimuthal position are generated and used to produce a three dimensional slope profile for a given optic. These circularity error-induced slope errors directly degrade the HPD of each shell.

A metric known as the delta-delta-radius (DDR), which describes differential radius variations, introduce local slope errors along the axial length of the shell. The DDR is derived from the circularity data and is used to calculate a representative HPD value for the shell. This HPD value is then used to compare the performance of the two shells: 62mm-S02 and 62mm-S03. Figure 7 shows the 62mm-S02 shell under test. Figure 8 shows the circularity data for both shells for a given scan, with 5 scans made per shell. 62mm-S02 circularity resulted in a 3.42" ± 1.24" DDR HPD while 62mm-S03 circularity resulted in a 4.08" ± 0.36" DDR HPD. These results show marginal improvement in overall performance of full shells utilizing Au release layer compared to the passivation layer. Other diagnostics including X-ray testing could further validate this result.

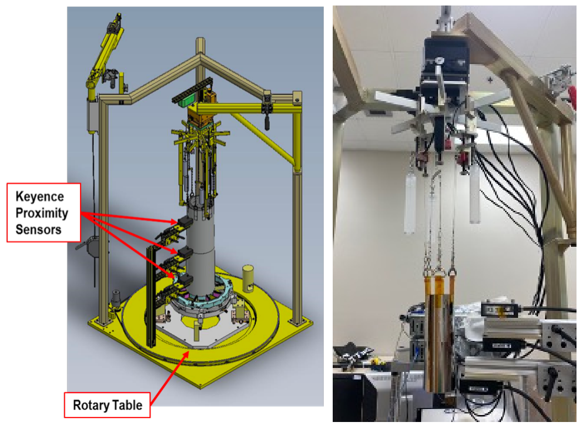

Figure 7: Left: Schematic of alignment station setup used for circularity testing of 62mm-S02 and S03. Right: Photo of S02 under test in circularity station.

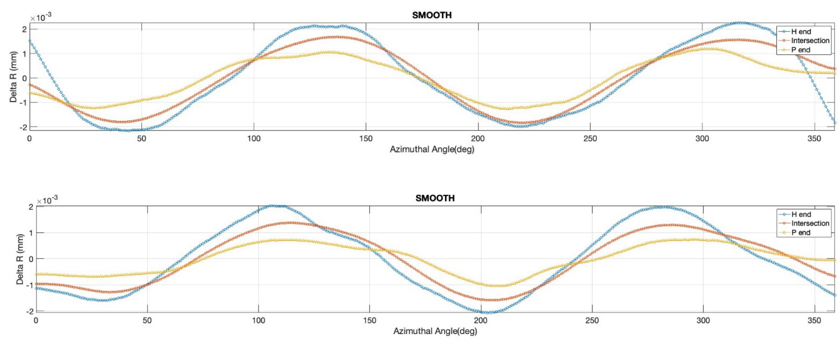

Figure 8: Circularity data taken from circularity station measurements for S02 (top) and S03 (bottom) used to calculate the DRR and consequent HPD values or each optic.

3.2 X-ray Testing

X-ray testing offers a more repeatable measure of the shell circularity and, therefore, could constrain the previous results further. Both shells, 62mm-S02 and 62mm-S03, were measured at MSFC's 100m beamline[24] using a Mo Tube with applied voltage of 10 kV and current of 1mA. Both shells were measured at a defocus of 40 mm and 0 degree up clocking angle in order to derive the circularity-induced error in the HPD. The resulting out-of-focus images are shown in Figure 9. The peak intensity within the out of focus image is identified and plotted as pixel distance from the average image radius. These data are then fit with a high-order polynomial from which a Fourier transform analysis is performed to derive the HPD. Figure 10 shows these data and their corresponding fits. Using this method, the calculated HPDs for 62mm-S02 and 62mm-S03 are 3.71" and 4.40", respectively. Repeat measurements of these optics in this configuration will help to constrain this result and inform the significance of this improvement.

Further testing at a range of clocking angles within the beamline will also further constrain these results. Additionally, poor surface roughness of the mandrel has resulted in less than optimal in-focus and defocus X-ray images, making the above analysis more difficult. A higher quality mandrel is currently being sourced and will be used to repeat this study and provide more clarification on the impact of the Au release layer on overall optic figure and performance.

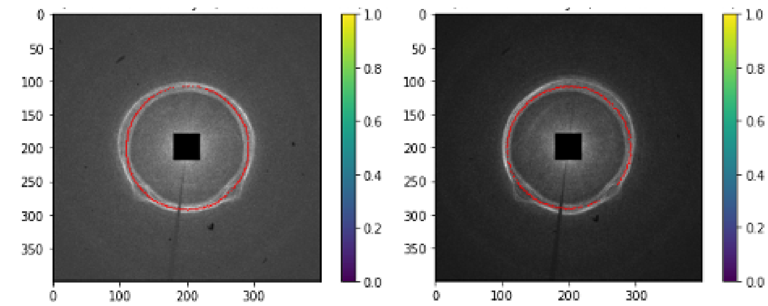

Figure 9: Defocus X-ray images taken at 40 mm from focal plane for 62mm-S02 (left) and 62mm-S03 (right)

4. SUMMARY AND FUTURE WORK

Au release layer development is under way at MSFC with the goal of improving overall imaging performance of full shell replicated NiCo optics for current and future missions. Comparative studies of release layer adhesion strengths for both the traditional passivation layer and optimized Au layer were conducted on flat coupon substrates as a proof-of-concept for pursuing Au release layers to reduce release-induced distortions.

Optimized Sputtered Au release layers were deposited onto a small-scale mandrel from which a 350 μm NiCo shell was fabricated. The resulting shell was compared to an identical one fabricated with the passivation layer. Circularity measurements utilizing a custom circularity station were conducted on both optics to assess if local slope errors from non-circularity in the azimuthal reference were reduced due to the lower-adhesion Au release layer. The derived HPD values for the Au release layer shell, 62mm-S02, and the passivated layer shell, 62mm-S03, were 3.42" $\pm$ 1.24" and 4.08" $\pm$ 0.36", respectively. Repeat tests are planned to improve statistics and help inform future Au release layer development.

X-ray tests were also performed on 62mm-S02 and -S03 to further investigate release layer impact on optical performance of full shell optics. The two shells were imaged at a defocus of 40 mm at 0 deg up orientation. These defocused ring images were analyzed and HPDs due to non-circularity errors were derived. An HPD of 3.71" was calculated for 62mm-S02, and an HPD of 4.40" was calculated for 62mm-S03. Repeat measurements as well as additional measurements at other clocking angles will help constrain these initial results.

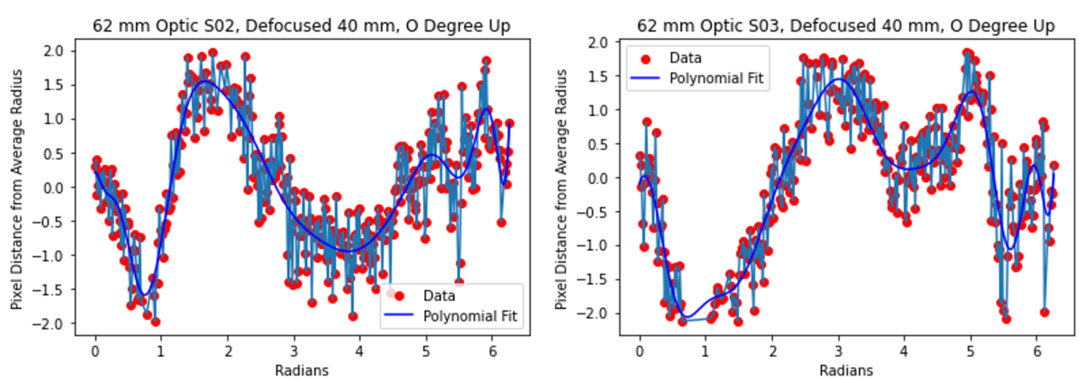

Figure 10: Defocus data derived from 40 mm out of focus x-ray images for 62mm-S02 (left) and 62mm-S03 (right).

Plans to test Au release layers on a higher quality, small-scale mandrel are in development with the goal of constraining measurement errors to quantify how the Au release layer can improve full shell optic performance. Future work will also include developing and testing Au release layers for flight-like, larger mandrels, such as those used for IXPE optics. At-scale testing of this method is critical to the comprehensive understanding and improvement of the full shell replication process.

ACKNOWLEDGMENTS

D.N.G would like acknowledge funding for this work through the NASA Astrophysics Division Internal Scientist Funding Model (ISFM) via NASA contract 80NSSC25K7330. The authors would also like to acknowledge the assistance of Dr. Suzanne Romaine and Riccardo Bruni from the Smithsonian Astrophysical Observatory (SAO) Center for Astrophysics (CfA) for their assistance with fabricating several Au coatings as well as providing the use of a 62 mm mandrel. K.P.D. would like to acknowledge support for this work through an appointment to the NASA Postdoctoral Program at NASA MSFC, administered by Oak Ridge Associated Universities under contract with NASA.

REFERENCES

[1] Ramsey, B. D., Alexander, C. D., Apple, J. A., Austin, R. A., Benson, C. M., Dietz, K. L., Elsner, R. F., Engelhaupt, D. E., Kolodziejczak, J. J., O'Dell, S. L., Speegle, C. O., Swartz, D. A., Weisskopf, M. C., and Zirnstein, G., "HERO: high-energy replicated optics for a hard-x-ray balloon payload," in [*X-Ray Optics, Instruments, and Missions IV*], Hoover, R. B. and II, A. B. C. W., eds., **4138**, 147 – 153, International Society for Optics and Photonics, SPIE (2000).

[2] Christe, S. D., Shih, A., Rodriguez, M., Cramer, A., Gregory, K., Edgerton, M., Gaskin, J., Wilson-Hodge, C., Apple, J., Chavis, K. S., Jackson, A., Smith, L., Dietz, K., O'Connor, B., Sobey, A., Koehler, H., and Ramsey, B., "The high energy replicated optics to explore the sun mission: a hard x-ray balloon-borne telescope," in [*Solar Physics and Space Weather Instrumentation V*], Fineschi, S. and Fennelly, J., eds., **8862**, 886206, International Society for Optics and Photonics, SPIE (2013).

[3] Glesener, L., Krucker, S., Christe, S., nosuke Ishikawa, S., Buitrago-Casas, J. C., Ramsey, B., Gubarev, M., Takahashi, T., Watanabe, S., Takeda, S., Courtade, S., Turin, P., McBride, S., Shourt, V., Hoberman, J., Foster, N., and Vievering, J., "The FOXSI solar sounding rocket campaigns," in [*Space Telescopes and Instrumentation 2016: Ultraviolet to Gamma Ray*], den Herder, J.-W. A., Takahashi, T., and Bautz, M., eds., **9905**, 99050E, International Society for Optics and Photonics, SPIE (2016).

[4] Baumgartner, W. H., Bongiorno, S., Kolodziejczak, J., Singam, S., Gurgew, D., Speegle, C., Banks, D., Champey, P., Thomas, N., and Davis, C. G., "High resolution full shell replicated x-ray optics for FOXSI-4," in [*Optics for EUV, X-Ray, and Gamma-Ray Astronomy XI*], O'Dell, S. L., Gaskin, J. A., Pareschi, G., and Spiga, D., eds., **12679**, 126790C, International Society for Optics and Photonics, SPIE (2023).

[5] Pavlinsky, M., Levin, V., Akimov, V., Krivchenko, A., Rotin, A., Kuznetsova, M., Lapshov, I., Tkachenko, A., Krivonos, R., Semena, N., Buntov, M., Glushenko, A., Arefiev, V., Yaskovich, A., Grebenev, S., Sazonov, S., Lutovinov, A., Molkov, S., Serbinov, D., Kudelin, M., Drozdova, T., Voronkov, S., Sunyaev, R., Churazov, E., Gilfanov, M., Ramsey, B., O'Dell, S. L., Kolodziejczak, J., Zavlin, V., and Swartz, D., "ART-XC / SRG overview," in [*Space Telescopes and Instrumentation 2018: Ultraviolet to Gamma Ray*], den Herder, J.-W. A., Nikzad, S., and Nakazawa, K., eds., **10699**, 106991Y, International Society for Optics and Photonics, SPIE (2018).

[6] Ramsey, B. D., Attina, P., Baldini, L., Barbanera, M., Baumgartner, W. H., Bellazzini, R., Bladt, J., Bongiorno, S. D., and et al., "The Imaging X-Ray Polarimetry Explorer (IXPE): technical overview IV," in [*UV, X-Ray, and Gamma-Ray Space Instrumentation for Astronomy XXII*], Siegmund, O. H., ed., **11821**, 118210M, International Society for Optics and Photonics, SPIE (2021).

[7] Singam, S. P., Gaksin, J., Kolodziejczak, J., Speegle, C., Bongiorno, S., Baumgartner, W., Davis, J., Thomas, N., Champey, P., Gurgew, D., Davis, C., and Ramsey, B., "Recent advancements in full-shell X-ray optics at MSFC," in [*AAS/High Energy Astrophysics Division*], *AAS/High Energy Astrophysics Division* **20**, 103.34 (Sept. 2023).

[8] Kolodziejczak, J., Gaskin, J., Baumgartner, W., Bongiorno, S., Champey, P., Gurgew, D., Ramsey, B., Singam, S. P., Speegle, C., and Thomas, N., "Achieving large-scale, high-resolution, full-shell replicated x-ray optics: budgeting for sources of angular-resolution errors," in [*Optics for EUV, X-Ray, and Gamma-Ray Astronomy XI*], O'Dell, S. L., Gaskin, J. A., Pareschi, G., and Spiga, D., eds., **12679**, 126791D, International Society for Optics and Photonics, SPIE (2023).

[9] Engelhaupt, D. E., Ramsey, B. D., O'Dell, S. L., Jones, W. D., and Russell, J. K., "New alloys for electroformed replicated x-ray optics," in [*X-Ray Optics, Instruments, and Missions IV*], Hoover, R. B. and II, A. B. C. W., eds., **4138**, 154 – 163, International Society for Optics and Photonics, SPIE (2000).

[10] Ramsey, B. D., Elsner, R. F., Engelhaupt, D. E., O'Dell, S. L., Speegle, C. O., and Weisskopf, M. C., "Development of hard x-ray optics at MSFC," in [*X-Ray and Gamma-Ray Telescopes and Instruments for Astronomy*], Truemper, J. E. and Tananbaum, H. D., eds., **4851**, 631 – 638, International Society for Optics and Photonics, SPIE (2003).

[11] Atkins, C., Ramsey, B., Kilaru, K., Gubarev, M., O'Dell, S., Elsner, R., Swartz, D., Gaskin, J., and Weisskopf, M., "X-ray optic developments at NASA's MSFC," in [*Damage to VUV, EUV, and X-ray Optics IV; and EUV and X-ray Optics: Synergy between Laboratory and Space III*], Juha, L., Bajt, S., London, R., Hudec, R., and Pina, L., eds., **8777**, 87770W, International Society for Optics and Photonics, SPIE (2013).

[12] Egle, W., Bulla, H., Kaufmann, P., Aschenbach, B., and Brauninger, H., "Production of the first mirror shell for the European Space Agency's XMM telescope by application of a dedicated large area replication technique," *Optical Engineering* **29**, 1267–1272 (Oct. 1990).

[13] Lumb, D. H., Jansen, F. A., and Schartel, N., "X-ray Multi-mirror Mission (XMM-Newton) observatory," *Optical Engineering* **51**(1), 011009 (2012).

[14] Sironi, G., Spiga, D., Pareschi, G., Missaglia, N., and Paganini, L., "Thin gold layer in Ni electroforming process: optical surface characterization," in [*Optics for EUV, X-Ray, and Gamma-Ray Astronomy IV*], O'Dell, S. L. and Pareschi, G., eds., **7437**, 743718, International Society for Optics and Photonics, SPIE (2009).

[15] Sironi, G., Spiga, D., Raimondi, L., Pareschi, G., Orlandi, A., Borghi, G., Missaglia, N., and Negri, B., "Thin gold layer in NiCo and Ni electroforming process: optical surface characterization," in [*Space Telescopes and Instrumentation 2010: Ultraviolet to Gamma Ray*], Arnaud, M., Murray, S. S., and Takahashi, T., eds., **7732**, 77322R, International Society for Optics and Photonics, SPIE (2010).

[16] Liao, Q., Wang, B., Ding, F., Li, D., Liu, W., Wang, L., Yang, Y., and Chen, Y., "Multiscale design and application of low adhesion strength dlc release layer," *Journal of Materials Research and Technology* **26**, 9518–9531 (2023).

[17] Romaine, S., Boike, J., Bruni, R., Engelhaupt, D., Gorenstein, P., and Ramsey, B., "Improved release coatings for electroformed x-ray optics," in [*Optics for EUV, X-Ray, and Gamma-Ray Astronomy V*], O'Dell, S. L. and Pareschi, G., eds., **8147**, 81470W, International Society for Optics and Photonics, SPIE (2011).

[18] Gurgew, D. N., Broadway, D. M., and Ramsey, B. D., "Direct current magnetron coating chamber characterization directed toward the efficient development of broadband x-ray optic multilayer coatings," *Journal of Astronomical Telescopes, Instruments, and Systems* **6**, 015004 (Jan. 2020).

[19] Windt, D., "IMD—Software for modeling the optical properties of multilayer films," *Computers in Physics and IEEE Computational Science and Engineering* **12**, 360–370 (July 1998).

[20] Gurgew, D. N., Broadway, D., Gubarev, M., and Ramsey, B., "Design and implementation of an x-ray reflectometer system for testing x-ray optics coatings," in [*Society of Photo-Optical Instrumentation Engineers (SPIE) Conference Series*], *Society of Photo-Optical Instrumentation Engineers (SPIE) Conference Series* **9603**, 96031S (Sept. 2015).

[21] DeFelsko Inspection Instruments, "Defelsko PosiTest AT."

[22] Gurgew, D. and Singam, S. P., "Characterization of NiC multilayer coating stress for x-ray optic applications," in [*Optics for EUV, X-Ray, and Gamma-Ray Astronomy XI*], **12679**, 126790N, International Society for Optics and Photonics, SPIE (2023).

[23] Bongiorno, S. D., Baumgartner, W. H., Kolodziejczak, J., Davis, C. G., Ranganathan, J., Thomas, N., McCracken, J., and Gurgew, D., "Assembly of the FOXSI-4 mirror modules," in [*Optics for EUV, X-Ray, and Gamma-Ray Astronomy XI*], O'Dell, S. L., Gaskin, J. A., Pareschi, G., and Spiga, D., eds., **12679**, 126790D, International Society for Optics and Photonics, SPIE (2023).

[24] Thomas, N. E., Baumgartner, W. H., Bongiorno, S. D., Champey, P. R., Cheney, S. P., Davis, C. G., Gaskin, J. A., Kolodziejczak, J., Singam, P., and Smith, D. D., "The Marshall 100-meter x-ray beamline," in [*Optics for EUV, X-Ray, and Gamma-Ray Astronomy XI*], O'Dell, S. L., Gaskin, J. A., Pareschi, G., and Spiga, D., eds., **12679**, 126790U, International Society for Optics and Photonics, SPIE (2023).